Rubisco proton production drives the elevation of CO_2 within condensates and carboxysomes

Authors:	**ORCID**	**ResearcherID**
Benedict M. Long [a,b,1]	0000-0002-4616-2967	B-3799-2008
Britta Förster [b]	0000-0002-5231-0954	O-7908-2015
Sacha B. Pulsford [b]		
G. Dean Price [a,b]	0000-0001-5906-4912	C-9505-2009
Murray R. Badger [a,b]		

Affiliations:

[a] Realizing Increased Photosynthetic Efficiency (RIPE); and [b] Australian Research Council Centre of Excellence for Translational Photosynthesis

Plant Science Division
Research School of Biology
The Australian National University
134 Linnaeus Way
Acton ACT 2601
AUSTRALIA

[1]Correspondence to: ben.long@anu.edu.au

ABSTRACT

Membraneless organelles containing the enzyme Ribulose-1,5-bisphosphate carboxylase/oxygenase (Rubisco), formed via liquid-liquid phase separation, are a common feature of organisms utilizing CO_2 concentrating mechanisms (CCMs). In cyanobacteria and proteobacteria, the Rubisco condensate is encapsulated in a proteinaceous shell, collectively termed a carboxysome, while microalgae have evolved liquid-like Rubisco condensates known as pyrenoids. In both cases, CO_2 fixation is enhanced compared with the free enzyme. Previous mathematical models have attributed the function of carboxysomes to the generation of elevated CO_2 within the organelle via a co-localized carbonic anhydrase (CA), and inwardly diffusing HCO_3^-. Here we present a novel concept in which we consider the net of two protons produced in every Rubisco carboxylase reaction, and have evaluated this in a reaction-diffusion, compartment model to investigate functional advantages of Rubisco condensation and how these may lead to carboxysome evolution. Applying diffusional resistance to reaction species within a modelled condensate allows Rubisco-derived protons to drive the conversion of HCO_3^- to CO_2 via co-condensed CA, enhancing both localized [CO_2] and Rubisco rate. Protonation of RuBP and PGA plays an important role in modulating internal pH and CO_2 generation. Application of the model to potential evolutionary intermediate states prior to contemporary carboxysomes revealed photosynthetic enhancements along a logical sequence of advancements, via Rubisco condensation, to fully-formed carboxysomes. Our model suggests that evolution of Rubisco condensation could be favored under low CO_2 and low light environments.

INTRODUCTION

42 Global atmospheric CO_2 capture into the biosphere has occurred over geological timescales primarily via the enzyme ribulose-1,5-bisphosphate carboxylase/oxygenase (Rubisco). Rubisco is
44 distinguished by the competitive inhibition of its carboxylation activity by molecular oxygen, leading to photorespiratory loss of CO_2 and metabolic energy (1). Possibly the most abundant protein on the
46 planet (2), Rubisco's competing catalytic activities have required evolution of the enzyme, and/or its associated machinery, to maintain capture of sufficient carbon into organic molecules to drive life on
48 Earth. The evolution of oxygenic photosynthesis ≈2.4 billion years ago has transformed the atmosphere from one rich in CO_2 and depleted of O_2 to one in which the relative abundances of these gases has
50 overturned (3). Under these conditions, the Rubisco oxygenation reaction has increased, to the detriment of CO_2 capture. This catalytic paradox has led to different adaptive solutions to ensure effective rates
52 of photosynthetic CO_2 fixation including; the evolution of the kinetic properties of the enzyme (4), increases in protein abundance in the leaves of many terrestrial C_3 plants (5) and, the evolution of
54 diverse and complex CO_2 concentrating mechanisms (CCMs) in many cyanobacteria, algae, and more recently hornworts, CAM, and C_4 plants (6, 7).

56 A defining characteristic of contemporary cyanobacteria is the encapsulation of their Rubisco enzymes within specialized bacterial micro-compartments called carboxysomes (8). These microbodies
58 are central to the cyanobacterial CCM, in which cellular bicarbonate (HCO_3^-) is elevated by a combination of membrane-associated HCO_3^- pumps and CO_2-converting complexes (9-11), to drive
60 CO_2 production within the carboxysome by an internal carbonic anhydrase (CA; 12, 13). This process results in enhanced CO_2-fixation, and is a proposed evolutionary adaptation to a low CO_2 atmosphere
62 (14, 15).

An analogous CCM operates in many microalgal species which contain chloroplastic Rubisco
64 condensates called pyrenoids (16). The microalgal CCM accumulates HCO_3^- and converts it to CO_2 within the pyrenoid to maximize CO_2-fixation. Common to both cyanobacterial and microalgal systems
66 is the presence of unique Rubisco-binding proteins, enabling liquid-liquid phase separation (LLPS) of Rubisco from the bulk cytoplasm (17-24). Condensation of proteins to form LLPS compartments within
68 the cell is an increasingly apparent means by which cellular processes can be segregated and organized, across a broad range of biological systems (25-27). The commonality of pyrenoid and carboxysome
70 function (28) despite their disparate evolutionary histories (6), suggest a convergence of function driven by Rubisco condensation.

72 We consider here that co-condensation of Rubisco and CA enzymes is beneficial for the elevation of internal CO_2 because Rubisco carboxylation produces a net of two protons for every reaction turnover
74 (Fig. S1; 29, 30). These protons can be used within the condensate to convert HCO_3^- to CO_2, with CO_2 being elevated (and pH lowered) as a result of restricted outward diffusion due to the high concentration

of protein in the condensate and surrounding cell matrix. We propose that proton release within a primordial Rubisco condensate enabled the evolution of carboxysomes with enhanced carboxylation rates.

RESULTS

The modelling of free Rubisco and Rubisco compartments

To demonstrate the feasibility of our proposal we initially consider a model of free Rubisco, a Rubisco condensate, and a carboxysome based on a set of compartmentalized reactions described in Fig. 1 and associated tables of parameters (Table 1, Table 2). The novel aspects of this model are; the inclusion of the production of protons by the Rubisco carboxylation and oxygenation reactions (and their equilibration across the carboxysome shell by free diffusion) and, proton movement via protonated RuBP and PGA species. These details of the model are new, but the other aspects of the model are similar to carboxysome models previously considered by others (9, 31-39).

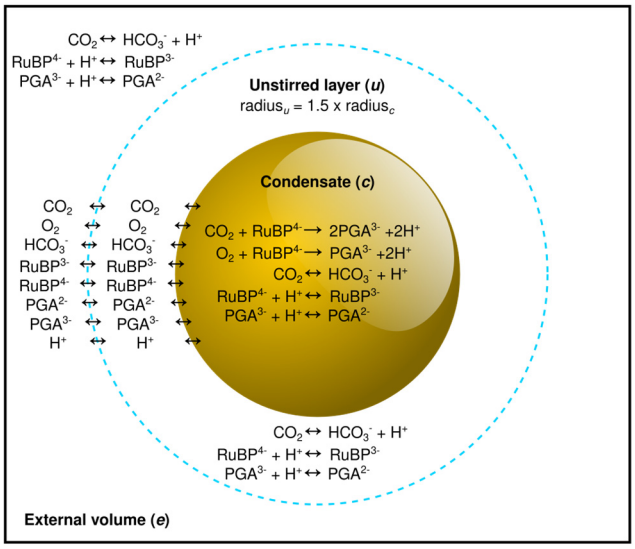

Fig. 1. Rubisco compartment model

A visual description of the compartment model used in this study. The model consists of three reaction compartments. The external compartment (*e*) represents the cellular cytoplasm in which inorganic carbon (C_i) species (CO_2 and HCO_3^-), along with RuBP and PGA, can undergo reversible reactions with protons (H^+). Interconversion of C_i species is catalyzed by carbonic anhydrase (CA), whereas RuBP and PGA protonation/deprotonation is determined by the rate of conversion at physiological pH given *pKa* values of relevant functional groups (Fig. S1). The central compartment of the model is a Rubisco condensate (*c*) in which Rubisco carboxylation and oxygenation reactions occur, along with RuBP/PGA protonation and CA reactions. The external volume and a Rubisco condensate are separated by an unstirred boundary layer compartment (*u*) in which protonation and CA reactions can occur. The diffusion of all reaction species between each compartment can be set in the model to simulate either a free Rubisco enzyme, a Rubisco condensate, or a carboxysome as described in Table 1.

Table 1. Typical initial values used in the COPASI biochemical compartment model in this study

Parameter		Cellular compartment		
		External (*e*)	Unstirred layer (*u*)	Condensate (*c*)
Rubisco sites (mol/m^3)		absent	absent	10
Permeability (m/s) [a]	Free Rubisco scenario	n/a	1	1
	Condensate scenario	n/a	1×10^{-4}	1×10^{-4}
	Carboxysome scenario	n/a	1×10^{-4}	1×10^{-6}
Carbonic anhydrase catalysis factor [b]	Internal	1	1	1×10^{5}
	External	1×10^{5}	1×10^{5}	1
	Internal and external	1×10^{5}	1×10^{5}	1×10^{5}
Carbonic anhydrase rate constants [c]	$CO_2 \rightarrow HCO_3^- + H^+$		0.05	
	$HCO_3^- + H^+ \rightarrow CO_2$		100	
Compartment volume (m^3)		1	9.95×10^{-18}	4.19×10^{-18}
Species concentrations (mol/m^3)	HCO_3^-	0.01 – 25	[d]	[d]
	CO_2 (Rubisco substrate)	$0.001 \times [HCO_3^-]$	[d]	[d]
	O_2 (Rubisco substrate)	0.25 – 0.36	[d]	[d]
	H^+ (Rubisco product)	1×10^{-5} (pH 8.0)	[d]	[d]
	$RuBP^{4-}$ (Rubisco substrate)	1×10^{-3} – 10	[d]	[d]
	$RuBP^{3-}$	[d]	[d]	[d]
	PGA^{3-} (Rubisco product)	[d]	[d]	[d]
	PGA^{2-}	[d]	[d]	[d]

[a] – Permeabilities of the unstirred layer and condensate compartments are varied to simulate the free enzyme, condensate or carboxysome scenarios.
[b] – Carbonic anhydrase (CA) catalysis factor > 1 indicates presence of CA in that compartment.
[c] – CA rate constants were kept the same in all compartments.
[d] – Values determined from the model.

Protons derived from Rubisco reactions influence both condensate and carboxysome function

The influence of Rubisco proton production on the response of carboxylation rate and Rubisco compartment [CO_2] to external substrate supply (RuBP and HCO_3^-) is considered in Fig. 2. Here we assess model responses under sub-saturating substrate conditions where we observe greatest proton responses within the model (Fig. S2), and account for differential changes in the 'apparent' $K_M RuBP$ arising from decreased permeability to this substrate in condensates and carboxysomes (Fig. 2A; Fig. S4).

If we eliminate carboxylation-derived proton production within a Rubisco compartment in the model (zero protons; Fig. 2A), then proton-driven, CA-dependent CO_2 production within either a condensate or carboxysome becomes limited by the influx of protons from the external environment. With increasing compartment proton production per Rubisco carboxylation reaction (one and two protons; Fig. 2A), the CO_2 concentration is enhanced within a condensate, and even more so within a carboxysome, increasing Rubisco CO_2 fixation rates. Levels of CO_2 are further enhanced if more protons are able to be produced per Rubisco turnover (e.g. three protons in Fig. 2A). In contrast to a condensate or carboxysome, the free Rubisco enzyme is unaffected by proton production due to the absence of a compartment with associated diffusional limitations.

118 We also assessed the modelled responses of the free enzyme, its condensate, and carboxysomes to [RuBP] under sub-saturating HCO_3^- (1 mM; Fig. 2B). Again, proton production by Rubisco led to
120 increases in condensate and carboxysome [CO_2], despite relatively high external HCO_3^- supply, resulting in corresponding increases in Rubisco carboxylation rate.

122 In considering why these results are obtained, it is important to note that if the internal pH of a Rubisco compartment is assumed to be 8.0, then compartment free [H^+] is only 10 nM. In the Rubisco
124 compartment volume utilized in our model (≈4.2 x 10^{-18} m^3) this represents less than a single free proton, and means that the diffusional driving forces for proton exchange across the carboxysomal shell, for
126 example, are 10^4–10^6 -fold smaller than those driving CO_2, HCO_3^-, PGA and RuBP diffusion (which are in µM and mM ranges). Hence, inward H^+ diffusion will be rate-limiting depending on the
128 permeability of the compartment to protons. Therefore, other proton sources must provide substrate for the CA HCO_3^- dehydration reaction. The net outcome is that proton production by Rubisco
130 carboxylation within a diffusion-limited compartment leads to an improvement in carboxylation turnover, compared with the free enzyme (Fig. S5).

132 The model also shows an increase in carboxylation turnover resulting from the protons arising through oxygenation within in a carboxysome, although this appears negligible in a Rubisco condensate
134 (Fig. S6). This suggests that oxygenation can support an increased rate of carboxylation via proton release in a carboxysome. Notably, like the model of Mangan, Flamholz, Hood, Milo and Savage (35),
136 we find that carboxysome function does not require specific diffusional limitation to O_2 influx in order to reduce oxygenation.

Table 2. Rubisco catalytic parameters used in competition modelling

Rubisco source	k_{cat}^C [1/s]	k_{cat}^O [1/s]	K_MCO_2 [µM]	K_MO_2 [µM]	K_MRuBP [µM]	Substrate specificity factor ($S_{C/O}$)	Carboxylation efficiency (k_{cat}^C/K_MCO_2) [1/s/µM]	References
Tobacco	3.40	1.14	10.7	295	18.0	82	0.318	(56)
Synechococcus	14.4	1.22[a]	172	585[a]	69.9	40	0.084	(55, 57)
Cyanobium	9.40	1.42[b]	169	1400[b]	40.0	55	0.056	(15, 58)
Ancestral F1A	4.77	1.42	113	2010	40.0[c]	60	0.042	(15, 58)
Ancestral F1B	4.72	0.50	120	641	69.9[c]	50	0.039	(15, 55)
Chlamydomonas	2.91	0.61	3.30	422	19.0[d]	61	0.088	(59, 60)

[a] – The k_{cat}^O and K_MO_2 for *Synechococcus* Rubisco are from Occhialini, Lin, Andralojc, Hanson and Parry (57).
[b] – The k_{cat}^O of the *Cyanobium* enzyme was estimated using the *Prochlorococcus* K_MO_2 (15), and the published values of k_{cat}^C, K_MCO_2 and $S_{C/O}$ for *Cyanobium* (58) using $k_{cat}^O = [(k_{cat}^C \times K_MO_2)/S_{C/O}]/K_MCO_2$.
[c] – K_MRuBP values for Ancestral F1A and F1B enzymes are those of *Cyanobium* and *Synechococcus* respectively, from the references highlighted.
[d] – The K_MRuBP value for *Chlamydomonas* is from Zhu and Spreitzer (59) while all other values are from Spreitzer, Peddi and Satagopan (60).

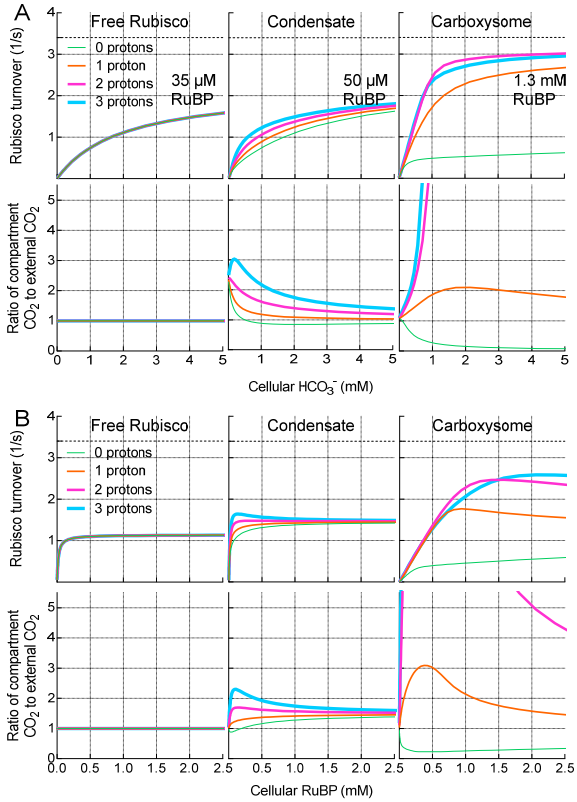

Fig. 2. Modelled responses of free Rubisco, condensate and carboxysome to external substrate supply

Modelled responses of free Rubisco, condensate and carboxysome to external HCO_3^- (A) and RuBP (B) supply. Carboxylation turnover rates (top panels) and the ratio of Rubisco compartment CO_2 to external CO_2 (lower panels) for the free enzyme, condensate and carboxysomes with zero, one, two or three protons being produced as products of the carboxylation reaction at sub-saturating RuBP (A) or HCO_3^- (B). Variation in permeabilities to RuBP between the free enzyme, condensate and carboxysome within the model result in increases in the apparent $K_M RuBP$ as permeabilities decline (Fig. S4). For HCO_3^- responses, the RuBP concentration used in each scenario is indicated. For RuBP responses, the HCO_3^- supply set at 1 mM [0.01 mM CO_2]). External CO_2 is set to 1/100 × external HCO_3^-. Net proton production by Rubisco carboxylation is theoretically two protons (Fig. 1). In all cases modelled rates include carbonic anhydrase (CA) activity only in the Rubisco compartment. Rubisco turnover in a carboxysome producing three protons/carboxylation drops below that of the two-proton system due a proton-driven shift in the $RuBP^{3-}$:$RuBP^{4-}$ ratio, decreasing the concentration of the Rubisco substrate species, $RuBP^{4-}$. Maximum carboxylation turnover rate (k_{cat}^C; 3.4 [1/s]) of the tobacco Rubisco used in this example (Table 2), is indicated by the *dashed line* in the upper panels. The COPASI (54) model was run in parameter scan mode, achieving steady-state values over the range of HCO_3^- concentrations indicated. Proton number was manufactured by modifying the Rubisco carboxylation reaction stoichiometry to produce zero, one, two or three protons in the model.

Carboxysome and condensate proton permeability

The diffusion of protons across the carboxysome envelope has been considered previously (40), but within the context that pH stabilization is entirely dependent upon free diffusion through the shell, and in the absence Rubisco activity which could lead to internally produced protons. Our proposal that the Rubisco reactions generate protons internally to the carboxysome requires a different set of considerations. Molecular simulations suggest that pores in the carboxysome shell favor negatively charged ions such as HCO_3^-, RuBP and PGA (41), and it is unlikely that the H_3O^+ ion will have entirely easy passage across the protein shell. For the diffusion of H_3O^+ in water, it is considered to have a higher diffusion rate than other ions in solution due to its participation in a proton wire system in collaboration

with water (42). For modelling purposes here, we have assumed that negatively charged ions have a permeability of 10^{-6} m/s across the carboxysome shell while H_3O^+ has a higher value of 10^{-4} m/s. The data in Fig. 3 show that proton permeability values greater than $\approx 10^{-5}$ m/s for the carboxysome shell leads to low carboxysome [CO_2] and lower Rubisco carboxylation turnover (under sub-saturating substrate supply).

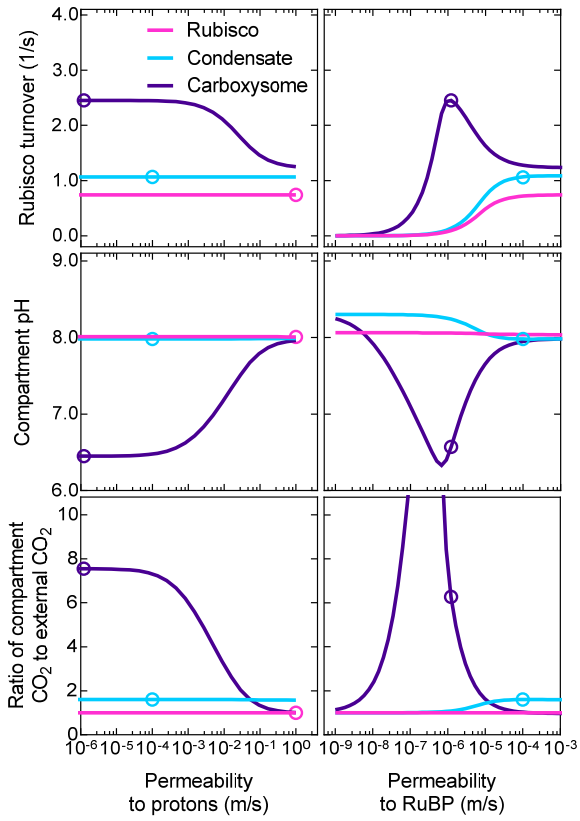

Fig. 3. Carboxysome and condensate function are dependent on proton and RuBP permeabilities

Rubisco carboxylation turnover (top panels), compartment pH (middle panels), and the ratio of Rubisco compartment CO_2 to external CO_2 (bottom panels) are dependent upon the permeability of the compartment to protons (left panels) and RuBP (right panels). Shown are modelled responses for free Rubisco (*pink lines*), a Rubisco condensate (*blue lines*), and a carboxysome (*purple lines*) at sub-saturating substrate concentrations (1 mM HCO_3^- [0.01 mM CO_2] and either 35, 50 or 1,300 μM RuBP for the free enzyme, condensate and carboxysome respectively; see Fig. 2 and Fig. S2). *Open circles* represent the values obtained for typical permeabilities used in the model (Table 1). Data were generated using the COPASI (54) model run in parameter scan mode, achieving steady-state values over the range of proton and RuBP permeabilities indicated for the Rubisco compartment. For all cases CA activity was only present within the Rubisco compartment. Data presented are for the tobacco Rubisco with parameters listed in Table 2.

Unlike the carboxysome, condensate proton permeability does not appear to modulate Rubisco carboxylation (Fig. 3). However, a pH-dependency of internal condensate [CO_2] is clearly apparent (Fig. S2). In the case of a condensate, $RuBP^{3-}$ is able to carry protons from outside to inside, and therefore provides protons required to convert HCO_3^- to CO_2. This can be observed within the model by varying RuBP permeability, with values above 10^{-6} m/s leading to increased compartment [CO_2],

186 and enhanced carboxylation (Fig. 3). Variation of condensate permeabilities to protons and RuBP shows that fluxes of reaction species across the condensate boundary are permeability-dependent (Fig. S3).

188

Roles for RuBP, PGA and CO_2 in Rubisco compartment pH

190 When we run the full model, including net proton production by Rubisco, carboxysome pH becomes acidic at limiting substrate concentrations as a result of limited proton efflux (Fig. 4). As
192 external substrate increases and internal CO_2 rises, the pH approaches that of the external medium (which we set to pH 8.0 with the initial H^+ concentration). Here, increasing CO_2 efflux from the
194 carboxysome is able to effectively dissipate protons from the Rubisco compartment, since there is a net loss of CO_2 that would otherwise be used for proton production by the CA hydration reaction (CO_2 +
196 $H_2O \leftrightarrow HCO_3^- + H^+$). This can be seen when we modify the rate of CO_2 efflux from the carboxysome by altering compartment CO_2 permeability. Slow CO_2 efflux leads to increased free proton
198 concentrations within the compartment, and fast efflux enables a return to approximately external pH as substrate supply increases (Fig. 4).

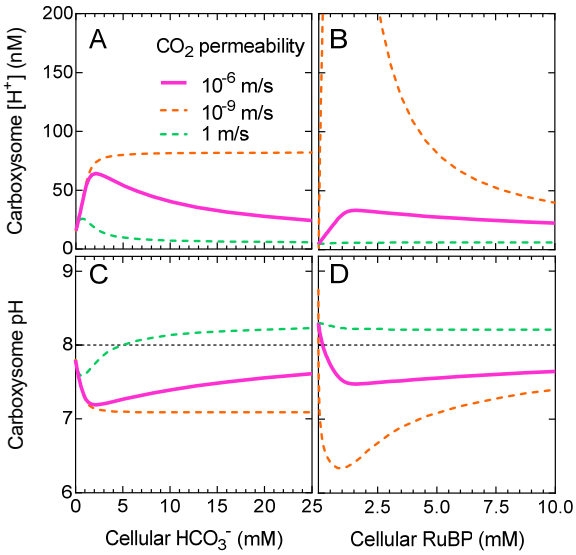

200

Fig. 4. Carboxysome proton concentration is modulated by CO_2 efflux

202 Carboxysome free proton concentration (A, B) and carboxysome pH (C, D) indicate that a functional carboxysome compartment undergoes net acidification at limiting HCO_3^- and RuBP supply (Fig. S2). Plotted are proton concentration and pH over a range
204 of [HCO_3^-] and [RuBP] for modelled carboxysomes with an internal carbonic anhydrase (CA), allowing for two protons to be produced per carboxylation reaction, and under typical modelled CO_2 permeability within the model (10^{-6} m/s; *solid pink lines*). If
206 CO_2 efflux were rapid and unimpeded (CO_2 permeability 1 m/s; *dashed green lines*), pH rapidly returns to ≈8 (*black dashed line*, panels C and D) as external limiting substrate supply increases. Slow CO_2 efflux (CO_2 permeability 10^{-9} m/s; *dashed orange lines*)
208 does not allow for dissipation of protons. Efflux of CO_2 from the carboxysome contributes to pH maintenance is it represents the loss of substrate for the CA hydration reaction ($CO_2 + H_2O \leftrightarrow HCO_3^- + H^+$), which would otherwise lead to free proton release.
210 Each dataset was modelled with an initial [RuBP] of 5 mM for HCO_3^- response curves, and 20 mM HCO_3^- in the case of RuBP response curves and CA activity is confined only to the carboxysome compartment. All other permeabilities under these conditions
212 are set to 10^{-6} m/s as for a carboxysome (Table 1). The COPASI (54) model was run in parameter scan mode, achieving steady-state values over a range of substrate concentrations. Data presented are for the tobacco Rubisco (Table 2).

When we consider reaction species' fluxes across the Rubisco compartment boundary, we find that both $RuBP^{3-}$ and PGA^{2-} can play a role in carrying protons out of both condensates and carboxysomes (Fig. 5), contributing to the stabilization of internal pH. In carboxysomes, $RuBP^{3-}$ and PGA^{2-} efflux plays a significant role in pH balance at very low HCO_3^-. However, as external HCO_3^- rises, carboxysome CO_2 efflux replaces RuBP and PGA as the major proton carrier (Fig. 5) as described above. For a condensate, CO_2 efflux is the primary means of stabilizing internal pH within the model over a range of HCO_3^- concentrations.

Similar responses can be seen over a range of RuBP concentrations, where CO_2 efflux also plays a dominant role as a proton efflux carrier in the condensate, while $RuBP^{3-}$ and PGA^{2-} efflux are the major contributors to shuttling protons out of the carboxysome (Fig. 5). These results highlight that the inclusion of RuBP and PGA as proton carriers is essential for the proper functioning of the carboxysome, so internal pH does not fall too low to maintain Rubisco activity (43).

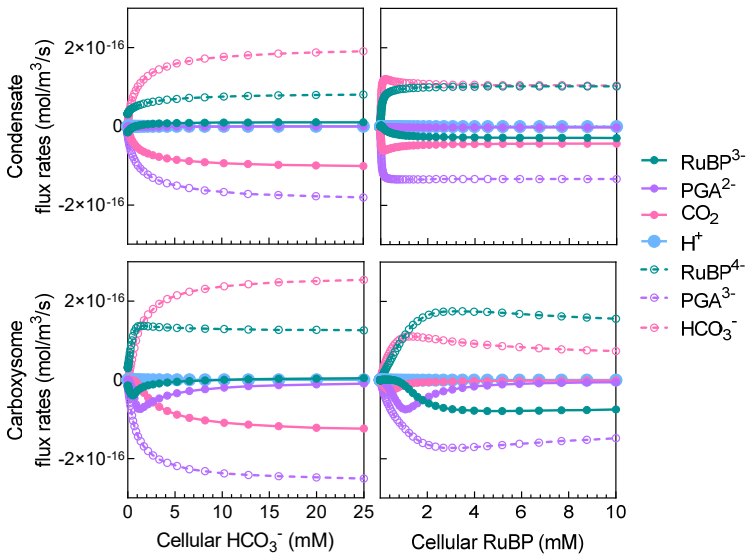

Fig. 5. Proton carriers help maintain compartment pH

Diffusional flux rates of chemical species across the condensate/carboxysome boundary over a range of HCO_3^- and RuBP concentrations in the model. Protons are carried by $RuBP^{3-}$, PGA^{2-} and CO_2 (as the substrate required for free proton release via the CA hydration reaction). Net free H^+ fluxes are extremely small and contributions to internal pH primarily arise through net fluxes of proton-carrier substrates (*solid circles*). The deprotonated $RuBP^{4-}$ and PGA^{3-} are the substrate and product of Rubisco carboxylation, respectively, within the model. Positive flux values indicate net influx into the compartment and negative values indicate net efflux. The COPASI (54) model was run in parameter scan mode, achieving steady-state at each substrate concentration. For HCO_3^- response curves, RuBP was set to 50 μM for a condensate and 1.3 mM for a carboxysome based on changes in apparent $K_M RuBP$ values arising from diffusional resistance (Fig. 2, Fig. S4). External $[HCO_3^-]$ was set to 1 mM for the generation of RuBP response curves. Data presented are for the tobacco Rubisco (Table 2) and model parameters for a condensate or a carboxysome are indicated in Table 1.

238 Model output also emphasizes that compartment pH is highly dependent on the buffering capacity of RuBP and PGA. Not only does RuBP carry protons released in Rubisco reactions, both species also
240 undergo protonation and deprotonation at physiological pH. Modifying their *pKa* values *in silico* significantly alters Rubisco compartment pH (Fig. S7).

242

The need for CA

244 In previous models of carboxysome function there is a need for CA to accelerate the conversion of HCO_3^- to CO_2 to support high rates of Rubisco CO_2 fixation and CO_2 leakage out of the carboxysome.
246 This is also true here, with internal interconversion needing acceleration to maximize Rubisco CO_2 fixation at saturating external HCO_3^- (Fig. S8). Additionally, we find that CA inclusion within a
248 condensate at high rates provides additional benefit to Rubisco carboxylation rates (Fig. S8).

It is also apparent that in the carboxysome CA function is dependent upon RuBP and HCO_3^-
250 supply, emphasizing that provision of protons from the Rubisco reaction is essential for the production of CO_2 from HCO_3^- via the CA enzyme (Fig. S9). This dependency appears to be much less in a
252 condensate due to much higher permeabilities of $RuBP^{3-}$ and CO_2 to the condensate interior (Fig. S8) and the low $K_M CO_2$ of the tobacco Rubisco modelled in this scenario.

254

Carboxysome evolution via Rubisco condensation

256 Noting improved function of Rubisco co-condensed with CA over its free enzyme counterpart utilizing our model (Fig. 2), and given the knowledge that Rubisco condensation underpins
258 carboxysome biogenesis (18, 24), we considered that the model may provide insights into carboxysome evolution via intermediate states utilizing Rubisco condensates.

260 To investigate this proposal, we analyzed the performance of potential evolutionary intermediates in a series of hypothesized pathways from free Rubisco to contemporary carboxysomes. We first
262 assumed a photorespiratory loss of ½ mole of CO_2 for every mole of O_2 fixed within the model, and by calculating average net carboxylation rates by each hypothesized evolutionary intermediate under
264 different atmospheric conditions (see Methods). This allowed relative fitness comparisons of proposed evolutionary states under what might reasonably be considered low or high atmospheric CO_2, as may
266 have been experienced under atmospheres where CCMs arose (7, 44). We assume here that a greater average net carboxylation rate for a particular evolutionary intermediate (over a given range of HCO_3^-)
268 would result in greater relative fitness and, therefore, evolutionary advantage. We apply this concept over HCO_3^- ranges within the model, rather than single-point comparisons, to provide a clearer view of
270 Rubisco responses resulting from variations in the observed response curves (Fig. S10).

We made these fitness calculations at both 20% and 30% O_2, to simulate alternative atmospheres under which CCMs may have arisen (7, 44). We calculated the average net carboxylation rates for the defined HCO_3^- ranges (see Methods), and generated phenotype matrices to allow comparison of possible evolutionary states (Fig. 6; Supplementary dataset S1). In evolutionary state comparisons, those states which lead to larger average net carboxylation rates were considered to have greater fitness.

The relative fitness of Form I Rubisco enzymes from a variety of sources were compared within the model, over all proposed evolutionary intermediates, to observe any differences resulting from varying Rubisco catalytic parameters (Table 2). A complete analysis of each Rubisco source and its performance at each proposed evolutionary step, under varied HCO_3^- and O_2 conditions is supplied in the Supplementary dataset S1.

Percent change in average net carboxylation rates - 20% O_2 0.01 - 1 mM cellular HCO_3^-		Next evolutionary state									
		Free Rubisco -CA	Free Rubisco +CA	Condensate +ext CA	Condensate +int/ext CA	Condensate +int CA	Carboxysome +int CA	Carboxysome +int/ext CA	Condensate -int/ext CA	Carboxysome -int/ext CA	Carboxysome +ext CA
Initial state	Free Rubisco -CA	0	0	21	165	126	273	273	-135	-281	-276
	Free Rubisco +CA	0	0	21	165	126	273	273	-135	-281	-276
	Condensate +ext CA	-17	-17	0	119	87	208	208	-129	-250	-246
	Condensate +int/ext CA	-62	-62	-54	0	-15	41	41	-113	-168	-166
	Condensate +int CA	-56	-56	-47	17	0	65	65	-115	-180	-178
	Carboxysome +int CA	-73	-73	-68	-29	-39	0	0	-109	-149	-147
	Carboxysome +int/ext CA	-73	-73	-68	-29	-39	0	0	-109	-149	-147
	Condensate -int/ext CA	389	389	449	865	753	1176	1177	0	-423	-408
	Carboxysome -int/ext CA	155	155	167	246	225	306	306	81	0	3
	Carboxysome +ext CA	157	157	169	251	228	312	312	80	-3	0

Fig. 6. Fitness matrix for proposed evolutionary steps from free Rubisco to contemporary carboxysomes

An example fitness matrix for the tobacco Rubisco enzyme showing percentage difference in average net Rubisco carboxylation rates (see Methods and Fig. S10) over a 0.01 – 1 mM HCO_3^- in a 20% O_2 atmosphere. Within this table an initial evolutionary state (*left, rows*) can be compared with any potential next evolutionary state (*top, columns*). Values are percent changes in average net carboxylation rates between each state. Positive (*yellow*) values indicate an improvement in average net Rubisco carboxylation turnover when evolving from an initial state to the next evolutionary state. Negative (*blue*) values indicate a net detriment. As an example, evolution from free Rubisco with associated carbonic anhydrase (Free Rubisco + CA) to a Rubisco condensate with an internal CA (Condensate + int CA) shows a 126% improvement in average net carboxylation turnover over. We assume that such an evolutionary adaptation would result in a competitive advantage over the initial state. Contrarily, a Rubisco condensate with both internal and external CA (Condensate +int/ext CA) shows a decrease in average net carboxylation turnover of 15% if the external CA was lost in an evolutionary adaptation (Condensate + int CA). Data presented here are for the tobacco Rubisco (Table 2), using the compartment model to simulate all potential evolutionary states (Table 1). The same pattern of potential evolutionary improvements is apparent regardless of the Rubisco source used in the model, assuming sufficient RuBP supply (Supplementary dataset S1).

Regardless of the type of Rubisco used in this analysis, the same pattern of potential evolutionary augmentations was favored (Fig. 6, Fig. 7, and Supplementary dataset S1). In all cases, condensation of Rubisco in the absence of a CA enzyme, as an initial evolutionary step ('Rubisco - CA' to 'Condensate – int/ext CA'; Fig. 6), resulted in a decrease in fitness, emphasizing that the starting point for the evolution of Rubisco condensates and carboxysomes likely began with a cellular CA present ('Rubisco + CA').

In Fig. 6 we provide an example evolutionary matrix for hypothesized progressions from a free Rubisco enzyme to a contemporary carboxysome. As a primary evolution, we speculated that

condensation of Rubisco could have occurred either with or without co-condensation of CA ('Condensate + int CA' or 'Condensate + ext CA'), or an alternate evolution where some CA was co-condensed and some remained in the external compartment ('Condensate + int/ext CA'). All three possibilities gave rise to condensates with improved fitness over the free enzyme (Fig. 6, Fig. 7, and Supplementary dataset S1). While the greatest improvement was calculated for a condensate with both internal and external CA ('Condensate + int/ext CA'), this state showed a negative transition in evolving to a condensate with only internalized CA ('Condensate + int CA').

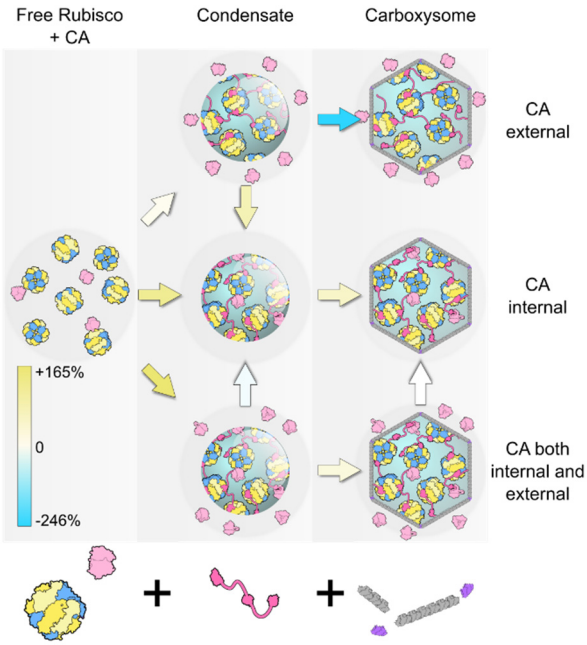

Fig. 7. Proposed evolution pathways to carboxysomes from free Rubisco via condensation

Model simulations propose condensation of Rubisco (*blue/yellow*) in the presence of a cellular carbonic anhydrase (CA) enzyme (*light pink*), here presented as three possible evolutionary alternatives with the CA external, internal, or both external and internal of the condensate. More detailed analysis shows that evolution of a Rubisco condensate in the absence of a CA is not feasible (Fig. 6). Condensation is proposed to occur through the evolution of a condensing protein factor (here CcmM from β-carboxysomes, *bright pink*), and carboxysome formation via the acquisition of bacterial microcompartment shell proteins (*grey, purple*). Contemporary carboxysomes are represented by those containing only internal CA. Percent increase or decrease in average net carboxylation rates between each proposed evolutionary intermediate is indicated by the colored arrows, and the color-scale indicates the values presented in Fig. 6. Between proposed evolutionary stages, *yellow-shaded* arrows indicate an improvement in average net carboxylation rate and *blue-shaded* arrows a net decrease, suggesting a loss in competitive fitness. No net change is indicated by a *white arrow*. The same pattern of potential evolutionary improvements is apparent regardless of the Rubisco source used in the model, assuming sufficient RuBP supply (Supplementary dataset S1).

Following initial condensate formation, we propose that the next probable advancement would be the acquisition of bacterial micro-compartment proteins (8) to form a shell with enhanced diffusional resistance. Within the model, only condensates with internalized CA enzymes ('Condensate + int CA' and 'Condensate + int/ext CA') displayed an improved CO_2 fixation phenotype during a single step acquisition of a carboxysome shell (Fig. 6, Fig. 7 and Supplementary dataset S1). There was no difference in fitness phenotype between carboxysomes with internal CA ('Carboxysome + int CA') and those with both internal and external CA ('Carboxysome +int/ext CA') in the model.

334 **Which Rubisco catalytic parameters correlate with evolutionary fitness?**

Applying the same evolutionary fitness analysis to the extant and extinct Rubiscos in our analysis
336 (Table 2), we were able to estimate the Rubisco catalytic properties that would make the most competitive advances through condensation and encapsulation. We determined correlation statistics for
338 the average net carboxylation turnover rates (1/s) under different atmospheres, and each catalytic parameter (Table 2), for the most likely evolutionary steps determined from the initial analysis (Fig. 7).
340 We draw the reader's attention to Supplementary dataset S1 and corresponding correlation plots in Fig. S11 to Fig. S15, where we present the data for the analysis presented in this section.

342 Regardless of the proposed step in the evolution toward contemporary carboxysomes (Fig. 7), the tobacco Rubisco, characterized by a high specificity ($S_{C/O}$) for CO_2 over O_2, and high carboxylation
344 efficiency ($k_{cat}^{C}/K_M CO_2$, 1/s/µM; Table 2), had the greatest average net carboxylation turnover rate at the low CO_2 range (0.01 – 1 mM cytoplasmic HCO_3^-; Fig. 8). This was observed under both high (30%)
346 and low (20%) O_2 atmospheres.

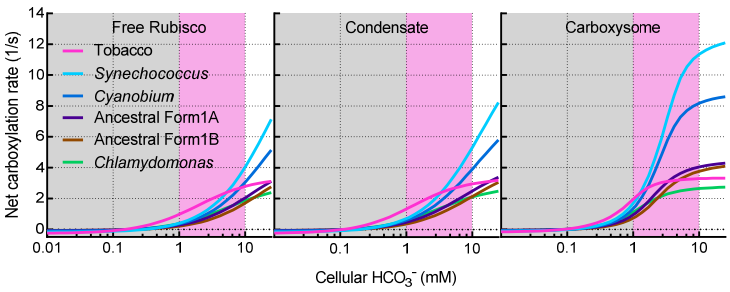

348 **Fig. 8. Net Rubisco carboxylation turnover rates in competing enzymes**

Net carboxylation turnover rates of competing Rubisco enzymes (Table 2) in the model as free enzymes, condensates or
350 carboxysomes. Each state was modelled using the parameters outlined in Table 1 and as described in the Methods. Rates are depicted under low (0.01 – 1 mM HCO_3^-; *grey shaded area*) and high (1 – 10 mM HCO_3^-; *pink shaded area*) CO_2 environments.
352 Data presented here are calculated under a 20% O_2 atmosphere.

354 Competitive fitness analyses at the high CO_2 range (1 – 10 mM cytoplasmic HCO_3^-; Fig. 8) indicated that the contemporary carboxysomal Rubisco from *Synechococcus* (characterized by low $S_{C/O}$,
356 high k_{cat}^{C}, high $K_M CO_2$, and high $K_M RuBP$, Table 2) performed best in all proposed evolutionary stages, regardless of atmospheric O_2, with the exception of free enzyme comparisons where it was out-
358 competed by the tobacco enzyme.

For the free enzyme ('Rubisco + CA') at both low CO_2 and low O_2, $S_{C/O}$ and $k_{cat}^{C}/K_M CO_2$
360 displayed strong positive correlations with the average net carboxylation rate (r = 0.855 – 0.986, p < 0.05). However, under low CO_2 and elevated O_2, while $S_{C/O}$ still correlated positively with average net

362 carboxylation rate (r = 0.828, p = 0.042), carboxylation turnover (k_{cat}^{C}) showed a strong negative correlation (r = -0.914, p = 0.011), indicating a selective pressure for high specificity and low catalytic
364 turnover for the free enzyme under elevated O_2. At elevated CO_2, there was no Rubisco parameter which correlated with average net Rubisco carboxylation rate, regardless of O_2 concentration.

366 For Rubisco condensates (with either internal, external, or both internal and external CA) correlations between average net carboxylation rate and Rubisco catalytic parameters were very similar
368 to the free enzyme. Again, under low CO_2 and low O_2, $S_{C/O}$ and $k_{cat}^{C}/K_M CO_2$ correlated positively with average net carboxylation turnover (r = 0.853 – 0.989, $p < 0.05$), the only exception being an apparent
370 negative correlation between net carboxylation and $K_M RuBP$ under these conditions for a condensate with an external CA (r = -0.829, p = 0.041). This implies that a Rubisco condensate with an external
372 CA would be under selective pressure to improve Rubisco RuBP utilization under low CO_2 and O_2.

At elevated O_2 and low CO_2, a condensate with an external CA appeared to show similar
374 dependencies on reduced k_{cat}^{C} and improved $S_{C/O}$ as the free enzyme. However, for condensates with internal CAs ('Condensate + int CA' and 'Condensate + int/ext CA'), net carboxylation correlated with
376 increased $S_{C/O}$ and $k_{cat}^{C}/K_M CO_2$ (r = 0.834 – 0.994, $p < 0.05$).

Like the free enzyme, there was no correlation between net carboxylation rates and any Rubisco
378 catalytic parameter for any condensate type at high CO_2, regardless of the O_2 concentration. This implies no selective pressure to evolve the Rubisco catalytic parameters analyzed under a high CO_2 environment
380 for either free Rubisco or Rubisco condensates.

Comparative analysis of different Rubisco enzymes in carboxysomes showed there was a strong
382 correlation between $k_{cat}^{C}/K_M CO_2$ and net carboxylation rates at low CO_2 (r = 0.885 – 0894, $p < 0.05$), regardless of O_2 concentration. At high CO_2 concentrations (the likely cellular environment for
384 contemporary carboxysomes in functional CCMs), k_{cat}^{C} was the only Rubisco catalytic parameter to correlate with net carboxylation rate in the model (r = 0.978 – 0.981, $p < 0.05$).

386

Low light may drive condensate evolution

388 Observing increased relative responses of compartment CO_2 to low RuBP concentrations in the model, where condensate pH is maximally decreased (Fig. S2), we assessed the relative fitness of
390 condensates at sub-saturating RuBP (50 µM) over HCO_3^- ranges in the model. Low cellular RuBP can generally be attributed to light-limited RuBP regeneration via the Calvin Cycle (45). A concentration
392 of 50 µM RuBP is approximately three-times the $K_M RuBP$ of the tobacco Rubisco used here (Table 2) and supports ≈63% of the CO_2-saturated rate for a condensed Rubisco (Fig. S4). At 50 µM RuBP we
394 observe enhanced net carboxylation turnover in the condensate compared with the free enzyme, especially at low HCO_3^- (Fig. S16). However, 50 µM RuBP is insufficient to support appreciable

396 carboxylation in a modelled carboxysome due to decreased substrate permeability (Fig. S4 and Fig. S16).

398

DISCUSSION

400 ### The functional advantages of a condensate/carboxysome

The modelling of both Rubisco condensates and carboxysomes in this study demonstrates a 402 number of factors which we predict play a key role in the function and evolution of these Rubisco "organelles". Firstly, the formation of a Rubisco condensate creates a localized environment in which 404 HCO_3^- can be converted to CO_2 in the presence of CA. CO_2 can be elevated relative to the external environment by the creation of a viscous unstirred protein solution boundary layer. The presence of 406 condensates or carboxysomes in prokaryotic cells or chloroplasts, where protein concentrations are high, would favor this (46, 47).

408 The condensation of Rubisco results in the co-localization of Rubisco-reaction protons. This enhances the potential to elevate CO_2 by driving both the conversion of HCO_3^- to CO_2 in the Rubisco 410 compartment, and decreasing compartment pH under certain conditions (Fig. S2). This role for protons is seen most clearly in carboxysomes where both CA and Rubisco activity are highly dependent on 412 proton production by the Rubisco reaction (Fig. 2, and Fig. S9). Rubisco condensates show a smaller enhancement by Rubisco proton production due to greater permeability to protonated RuBP and PGA, 414 but under conditions of low RuBP and low HCO_3^-, condensate pH can be lowered and CO_2 elevated (Fig. 2 and Fig. S2).

416 The modelling emphasizes that the exchange of protons between internal and external environments is probably independent of free proton or H_3O^+ diffusion. Instead, the exchange is 418 dominated by the movement of protonated RuBP and PGA (with *pKa*'s around 6.6), and efflux of CO_2 which consumes a proton internally (Fig. S3, Fig. 4 and Fig. 5).

420

The effects of Rubisco compartment pH and the relevance of sugar phosphate proton 422 carriers

By accounting for the pK_a of physiologically relevant functional groups on RuBP and PGA, the 424 model reveals that these species allow for sufficient ingress of protons into a Rubisco compartment to drive higher rates of carboxylation. This is because the concentration gradients for RuBP and PGA are 426 significantly high (in the mM range), compared with protons at pH 8.0 (in the nM range), enabling them to act as proton carriers in physiologically relevant concentrations. The sophisticated model of Mangan, 428 Flamholz, Hood, Milo and Savage (35) also considers the net production of a proton within the

carboxysome [i.e. consumption of one proton by the CA dehydration reaction and the generation of two
430 protons by Rubisco carboxylation]. Their model explains that high relative diffusion rates of protons are sufficient to ensure the appropriate steady-state differential between the cytosol and the
432 carboxysome interior consistent with function. However, analysis of viral capsid shells which have some similarity to the carboxysome icosahedral shell, suggest proton transfer may need to be mediated
434 by specific channels (48, 49). It is important to establish the real permeability of the carboxysome shell to the hydronium ion, and whether high rates of exchange are mediated by channels, proton wires or
436 shuttles linked to protonated sugar phosphates suggested here.

438 **Drivers of Rubisco compartment evolution**

Our evolution analysis suggests that $S_{C/O}$ is a likely key driver in determining fitness for the free
440 Rubisco enzyme under low CO_2 atmospheres (Fig. S11). Indeed, the tobacco enzyme, having the greatest $S_{C/O}$ (Table 2) displayed the best performance under all low CO_2 scenarios (Fig. 8).
442 Carboxylation efficiency is also an important driver in determining relative fitness under low O_2 atmospheres, for both the free enzyme and condensates (Fig. S11 – Fig. S14). Furthermore, this analysis
444 suggests that under increased atmospheric O_2 (as would have occured some 300 million years ago, when levels of O_2 rose and CO_2 fell; 14) there is selective pressure to reduce k_{cat}^{C} of the free enzyme (Fig.
446 S11). This suggest that ancestral cyanobacterial Rubisco may have had kinetics similar to the tobacco Form IB enzyme, implying relatively high photorespiration rates in pre-CCM cyanobacteria. Notably,
448 contemporary cyanobacteria appear to contain a full suite of photorespiratory genes (50), despite limited Rubisco oxygenase activity in modern carboxysomes (51).

450 Together, our evolution analysis suggests that a low CO_2 atmosphere may be a key driver in the initial formation of Rubisco condensates. At elevated CO_2, regardless of O_2 concentration, condensate
452 fitness is unconstrained by Rubisco catalytic parameters (Fig. S12 – Fig. S14). Carboxysome formation likely provided compartment conditions which enabled the evolution of Rubisco enzymes with higher
454 k_{cat}^{C}, but appear to be unconstrained by O_2 in the atmosphere (Fig. S15). Changes in atmospheric O_2 may have led to the selection of enzymes with better specificity, catalytic efficiency, and $K_M RuBP$
456 during intermediate stages of Rubisco condensate evolution (Fig. S12 – Fig. S14).

The relative response of Rubisco condensates to low RuBP supply suggests that low light may
458 also provide conditions conducive to condensate evolution. Low light generally leads to low RuBP (45). In the model such conditions lead to greater advantage of Rubisco condensates over complete
460 carboxysomes (Fig. S16). This highlights that elaborations on simple Rubisco condensation can be afforded through facilitated substrate supply or potential diffusion barriers other than carboxysome
462 formation. The association between pyrenoids and thylakoids, for example, suggests that luminal protons can possibly contribute towards the conversion of HCO_3^- to CO_2 (51), and allows the possibility

464 that the pyrenoid function may be enhanced by the combined action of both Rubisco and thylakoid generated protons. This result highlights alternative evolution of Rubisco compartments such as
466 pyrenoids which would provide enhancements exclusive of shell formation.

468 **Limitations of the model**

The model is designed as an idealized Rubisco compartment within a cellular environment. We
470 use a single 'condensate' of 1 μm in radius for the demonstration of condensate function, approximating a large pyrenoid (52). It does not include an 'extracellular' compartment from which the cytoplasmic
472 compartment can receive inorganic carbon via either diffusion or specific C_i pumps. We do not model the system as a functional CCM, holding a static equilibrium between C_i species in the system, rather
474 than a disequilibrium which occurs in cyanobacterial cells (53).

We do not apply a pH sensitivity to Rubisco catalysis in the model. This is both for simplicity
476 and to highlight that without pH modulation in the model we would see dramatic changes in pH. Previous models (35) apply the pH-dependency of Rubisco as established by Badger (43), as would be
478 applicable in this instance. We would expect to see a decrease in Rubisco activity in our model resulting from acidification or alkalization of the Rubisco compartment. However, we do not currently know how
480 a condensate or carboxysome might modulate pH changes in reality, and how these might affect the enzymes within it. We also do not model CO_2 and Mg^{2+} dependencies upon Rubisco activation (43),
482 which would be relevant considerations, especially at low CO_2 supply, from a physiological standpoint. These considerations may underpin mechanistic controls at low substrate supply within both
484 compartment types.

Importantly, we note that the permeabilities for diffusion across the compartment interfaces have
486 no physical measurements to support them. The values for carboxysomes are in line with previous models but it should be realized that these values have been derived from model analysis and not
488 independent physical measurements. The values assumed for condensates, although seeming reasonable and supporting a functional model, have not been physically established independently.

490

Conclusions

492 Accounting for proton production by Rubisco reactions, their utilization in the CA reaction, and their transport via RuBP and PGA, our model highlights a role for protons in Rubisco condensate and
494 carboxysome function and evolution. Application of our model to proposed evolutionary intermediate states prior to contemporary carboxysomes provides a hypothetical series of advancements, and suggest
496 that low CO_2 and low light environments may be key environmental drivers in the evolutionary

formation of Rubisco condensates, while increases in atmospheric O_2 may have played a role in Rubisco catalytic parameter selection. Our modelled outcomes are achieved through assumption of diffusional resistances to reaction species, which align well with previous models but remain to be determined experimentally. Taken together, our analysis provides insights into the function of phase-separated condensates of proton-driven enzyme reactions.

METHODS

Mathematical modelling

Modelling of Rubisco compartment scenarios and data output were carried out using the biochemical network simulation program COPASI (copasi.org), described by Hoops*, et al.* (54). COPASI (v4.25, build 207) was used to simulate reaction time-courses achieving steady-state conditions in a three-compartment model where reaction species are linked in a biochemical network (Fig. 1). For standard modelling conditions catalytic parameters of the tobacco Rubisco were used, while those of *C. reinhardtii*, *C. marinum* PCC7001 and *S. elongatus* PCC7942, and predicted ancestral Form IA and Form IB enzymes (15) were also used in evolutionary fitness analysis (Table 2). Michaelis-Menten rate equations were applied to Rubisco catalysis as dependent upon substrate and inhibitor concentrations within the Rubisco compartment. O_2 was applied as an inhibitor of the carboxylation reaction and CO_2 an inhibitor of oxygenation. The ordinary differential equations describing the model components can be found in the Supplementary Equations. Reactions, reaction species and model parameters can be found in Supplementary Table 1, Supplementary Table 2, and Supplementary Table 3 respectively.

Variation in compartment types (i.e. the free enzyme, a condensate, or a carboxysome) was simulated in the model by varying unstirred boundary and condensate permeabilities to all reaction species (Table 1). The permeabilities to $RuBP^{3-}$ and $RuBP^{4-}$ were assumed to be the same, as were those for PGA^{2-} and PGA^{3-}, and a single permeability value applied to either RuBP or PGA species. Proton production by carboxylation and oxygenation reactions was varied by adjusting the proton stoichiometry for either reaction (Supplementary Table 1 and Supplementary Equations). Protonation and deprotonation of RuBP and PGA in each compartment was enabled by assigning rate constants equivalent to their *pKa* values (Supplementary Table 3).

The size of the external compartment was set to 1 m^3 within the model, and both the Rubisco compartment and unstirred boundary layer volumes determined by setting the Rubisco compartment radius. For standard modelling procedures we used a spherical Rubisco compartment radius of 1×10^{-6} m^3 and the unstirred boundary layer volume was determined from a radius 1.5 × that of the Rubisco compartment. While this approach generates an extremely large condensate or carboxysome, akin to

contemporary pyrenoids, variation in the compartment size has no effect on the conclusions of the
532 modelled outcomes.

CO_2 concentration in the external compartment was set to 0.01 × external [HCO_3^-]
534 (Supplementary Equations). Interconversion between CO_2 and HCO_3^- was allowed to proceed in all compartments with rate constants of 0.05 for the forward reaction ($CO_2 \rightarrow HCO_3^- + H^+$), and 100 for
536 the back reaction ($HCO_3^- + H^+ \rightarrow CO_2$). CA contribution was enabled by applying a multiplying factor to each rate, such that a factor of 1 simulates the absence of CA. Typical CA multiplying factors for
538 each type of modelled compartment are listed in Table 1.

O_2 concentration in the model was typically set at 20% by assigning a concentration of 0.25 mM,
540 the water-soluble concentration at 25 °C. For simulations at 30% O_2, a concentration of 0.36 mM was used.

542 Steady-state reactions were initialized by setting the reactant concentrations in the external compartment and running the model to achieve steady-state. Initial pH was set at 8.0 using an external
544 compartment [H^+] of 1×10^{-5} mM. For saturating Rubisco substrate concentrations, initial [HCO_3^-] was set to 20 mM and [$RuBP^{4-}$] was set to 5 mM. Interconversion of $RuBP^{4-}$ and $RuBP^{3-}$ at *pKa* 6.7 and pH
546 8.0 results in ≈95% of all RuBP as the $RuBP^{4-}$ species.

Rubisco site concentrations were typically set to 10 mM. This value is similar to that calculated
548 for α- and β-carboxysomes (55) although higher than that estimated for pyrenoids (19). It is nonetheless a reasonable upper limit for the purposes of examining system responses within the model.

550

Evolution analysis

552 Hypothesized free enzyme, condensate or carboxysome evolutionary intermediates (Fig. 6) were generated and analyzed within the model using the parameters in Table 1, applying the catalytic
554 parameters of each Rubisco enzyme in Table 2. For each scenario the model was run over a range of [HCO_3^-] from 0.01 to 25 mM, at saturating RuBP (5 mM). Both carboxylation and oxygenation rates
556 were output for each scenario and converted to turnover numbers by accounting for active site concentrations within the model. Net carboxylation turnover rates (1/s) were calculated by assuming a
558 photosynthetic cost of ½ mole of CO_2 loss for each mole O_2 fixed (Fig. S10). Modelling was carried out at both 20% and 30% O_2 (Table 1). Performance comparisons of each hypothesized evolutionary
560 state were made for both low CO_2 (0.01 – 1 mM HCO_3^-) and high CO_2 (1 – 10 mM HCO_3^-) ranges by calculating the average net carboxylation rates for each scenario at each CO_2 range and O_2 concentration
562 (Fig. S10). Fitness comparisons were determined from the absolute differences in average net carboxylation rates between each modelled scenario (Fig. 6; Supplementary dataset S1). An additional

dataset was calculated for the tobacco Rubisco enzyme at 20% O_2 and 50 μM RuBP to determine compartment-type performance under conditions simulating low light.

Correlations between average net carboxylation rates (over specified modelled atmospheres) and Rubisco catalytic parameters (Table 2) for each proposed evolutionary state (Fig. 6; Fig. S11 – Fig. S15) were calculated as Pearson correlation statistics, with p values calculated as two-tailed distribution of calculated t-statistics (Supplementary dataset S1). In our results we highlight correlations where $p < 0.05$. For plotting purposes (Fig. S11 – Fig. S15) Rubisco catalytic parameters (Table 2) were normalized to the largest value in each parameter set and plotted against average net carboxylation rates.

AUTHOR CONTRIBUTIONS

M.R.B designed and developed the model. B.M.L. and B.F. carried out modelling experiments. B.M.L. and M.R.B generated the Figures. B.M.L. wrote the manuscript draft. B.M.L., B.F., S.B.P., G.D.P. and M.R.B. discussed, wrote and edited manuscript revisions.

ACKNOWLEDGEMENTS

This work is supported by a sub-award from the University of Illinois as part of the research project Realizing Increased Photosynthetic Efficiency (RIPE) that is funded by the Bill & Melinda Gates Foundation, Foundation for Food and Agriculture Research, and the U.K. Government's Department for International Development under grant number OPP1172157, and an award from The Australian Research Council, Centre of Excellence grant for Translational Photosynthesis (CE140100015) to M.R.B., G.D.P. We thank A. Long for enabling rapid processing of COPASI data output.

REFERENCES

1. F. A. Busch, Photorespiration in the context of Rubisco biochemistry, CO_2 diffusion and metabolism. *Plant J.* **101**, 919-939 (2020).
2. Y. M. Bar-On, R. Milo, The global mass and average rate of rubisco. *Proc. Natl. Acad. Sci. USA* **116**, 4738-4743 (2019).
3. P. M. Shih, Photosynthesis and early Earth. *Curr. Biol.* **25**, R855-R859 (2015).
4. G. G. Tcherkez, G. D. Farquhar, T. J. Andrews, Despite slow catalysis and confused substrate specificity, all ribulose bisphosphate carboxylases may be nearly perfectly optimized. *Proc. Natl. Acad. Sci. USA* **103**, 7246-7251 (2006).
5. J. Galmés *et al.*, Expanding knowledge of the Rubisco kinetics variability in plant species: environmental and evolutionary trends. *Plant, Cell Environ.* **37**, 1989-2001 (2014).
6. J. A. Raven, J. Beardall, P. Sanchez-Baracaldo, The possible evolution and future of CO_2-concentrating mechanisms. *J. Exp. Bot.* **68**, 3701-3716 (2017).
7. A. Flamholz, P. M. Shih, Cell biology of photosynthesis over geologic time. *Curr. Biol.* **30**, R490-R494 (2020).

8. B. D. Rae, B. M. Long, M. R. Badger, G. D. Price, Functions, compositions, and evolution of the two types of carboxysomes: polyhedral microcompartments that facilitate CO_2 fixation in cyanobacteria and some proteobacteria. *Microbiol. Mol. Biol. Rev.* **77**, 357-379 (2013).
9. L. Fridlyand, A. Kaplan, L. Reinhold, Quantitative evaluation of the role of a putative CO_2-scavenging entity in the cyanobacterial CO_2-concentrating mechanism. *BioSyst.* **37**, 229-238 (1996).
10. S.-I. Maeda, M. R. Badger, G. D. Price, Novel gene products associated with NdhD3/D4-containing NDH-1 complexes are involved in photosynthetic CO_2 hydration in the cyanobacterium, *Synechococcus* sp. PCC7942. *Mol. Microbiol.* **43**, 425-435 (2002).
11. G. D. Price, Inorganic carbon transporters of the cyanobacterial CO_2 concentrating mechanism. *Photosynthesis Res.* **109**, 47-57 (2011).
12. S. S. Cot, A. K. So, G. S. Espie, A multiprotein bicarbonate dehydration complex essential to carboxysome function in cyanobacteria. *J. Bacteriol.* **190**, 936-945 (2008).
13. C. de Araujo *et al.*, Identification and characterization of a carboxysomal γ-carbonic anhydrase from the cyanobacterium *Nostoc* sp. PCC 7120. *Photosynthesis Res.* **121**, 135-150 (2014).
14. M. R. Badger, D. Hanson, G. D. Price, Evolution and diversity of CO_2 concentrating mechanisms in cyanobacteria. *Funct. Plant Biol.* **29**, 161-173 (2002).
15. P. M. Shih *et al.*, Biochemical characterization of predicted Precambrian RuBisCO. *Nat. Commun.* **7**, 10382 (2016).
16. L. C. M. Mackinder, The *Chlamydomonas* CO_2-concentrating mechanism and its potential for engineering photosynthesis in plants. *New Phytol.* 10.1111/nph.14749, 10.1111/nph.14749 (2017).
17. T. Wunder, Z. G. Oh, O. Mueller-Cajar, CO_2-fixing liquid droplets: Towards a dissection of the microalgal pyrenoid. *Traffic* **20**, 380-389 (2019).
18. H. Wang *et al.*, Rubisco condensate formation by CcmM in β-carboxysome biogenesis. *Nature* **566**, 131-135 (2019).
19. E. S. Freeman Rosenzweig *et al.*, The eukaryotic CO_2-concentrating organelle is liquid-like and exhibits dynamic reorganization. *Cell* **171**, 148-162 e119 (2017).
20. L. C. M. Mackinder *et al.*, A repeat protein links Rubisco to form the eukaryotic carbon-concentrating organelle. *Proc. Natl. Acad. Sci. USA* **113**, 5958-5963 (2016).
21. T. Wunder, S. L. H. Cheng, S.-K. Lai, H.-Y. Li, O. Mueller-Cajar, The phase separation underlying the pyrenoid-based microalgal Rubisco supercharger. *Nat. Commun.* **9**, 5076 (2018).
22. T. Chaijarasphong *et al.*, Programmed ribosomal frameshifting mediates expression of the α-carboxysome. *J. Mol. Biol.* **428**, 153-164 (2016).
23. F. Cai *et al.*, Advances in understanding carboxysome assembly in *Prochlorococcus* and *Synechococcus* implicate CsoS2 as a critical component. *Life* **5**, 1141-1171 (2015).
24. L. M. Oltrogge *et al.*, Multivalent interactions between CsoS2 and Rubisco mediate α-carboxysome formation. *Nat. Struct. Mol. Biol.* 10.1038/s41594-020-0387-7 (2020).
25. S. F. Banani, H. O. Lee, A. A. Hyman, M. K. Rosen, Biomolecular condensates: organizers of cellular biochemistry. *Nat. Rev. Mol. Cell Biol.* **18**, 285 (2017).
26. A. A. Hyman, C. A. Weber, F. Jülicher, Liquid-liquid phase separation in biology. *Annu. Rev. Cell. Dev. Biol.* **30**, 39-58 (2014).
27. S. Alberti, Phase separation in biology. *Curr. Biol.* **27**, R1097-R1102 (2017).
28. B. D. Rae *et al.*, Progress and challenges of engineering a biophysical carbon dioxide-concentrating mechanism into higher plants. *J. Exp. Bot.* **68**, 3717–3737 (2017).
29. M. R. Harpel, F. C. Hartman, Facilitation of the terminal proton transfer reaction of ribulose 1,5-bisphosphate carboxylase/oxygenase by active-site Lys166. *Biochemistry* **35**, 13865-13870 (1996).
30. G. G. B. Tcherkez *et al.*, D_2O solvent isotope effects suggest uniform energy barriers in ribulose-1,5-bisphosphate carboxylase/oxygenase catalysis. *Biochemistry* **52**, 869-877 (2013).
31. L. Reinhold, M. Zviman, A. Kaplan, "Inorganic carbon fluxes and photosynthesis in cyanobacteria — a quantitative model" in Progress in Photosynthesis Research: Volume 4 Proceedings of the VIIth International Congress on Photosynthesis Providence, Rhode Island,

USA, August 10–15, 1986, J. Biggins, Ed. (Springer Netherlands, Dordrecht, 1987), 10.1007/978-94-017-0519-6_62, pp. 289-296.

32. L. Reinhold, M. Zviman, A. Kaplan, A quantitative model for inorganic carbon fluxes and photosynthesis in cyanobacteria. *Plant Physiol. Biochem.* **27**, 945-954 (1989).

33. L. Reinhold, R. Kosloff, A. Kaplan, A model for inorganic carbon fluxes and photosynthesis in cyanobacterial carboxysomes. *Can. J. Bot.* **69**, 984-988 (1991).

34. N. Mangan, M. Brenner, Systems analysis of the CO_2 concentrating mechanism in cyanobacteria. *eLife* 10.7554/eLife.02043, e02043 (2014).

35. N. M. Mangan, A. Flamholz, R. D. Hood, R. Milo, D. F. Savage, pH determines the energetic efficiency of the cyanobacterial CO_2 concentrating mechanism. *Proc. Natl. Acad. Sci. USA* **113**, E5354–E5362 (2016).

36. M. R. Badger, G. D. Price, J. W. Yu, Selection and analysis of mutants of the CO_2-concentrating mechanism in cyanobacteria. *Can. J. Bot.* **69**, 974-983 (1991).

37. J. M. McGrath, S. P. Long, Can the cyanobacterial carbon-concentrating mechanism increase photosynthesis in crop species? A theoretical analysis. *Plant Physiol.* **164**, 2247-2261 (2014).

38. G. D. Price, M. R. Badger, Isolation and characterization of high CO_2-requiring-mutants of the cyanobacterium *Synechococcus* PCC7942 : two phenotypes that accumulate inorganic carbon but are apparently unable to generate CO_2 within the carboxysome. *Plant Physiol.* **91**, 514-525 (1989).

39. G. D. Price, M. R. Badger, Expression of human carbonic anhydrase in the cyanobacterium *Synechococcus* PCC7942 creates a high CO_2-requiring phenotype : evidence for a central role for carboxysomes in the CO_2 concentrating mechanism. *Plant Physiol.* **91**, 505-513 (1989).

40. B. B. Menon, S. Heinhorst, J. M. Shively, G. C. Cannon, The carboxysome shell is permeable to protons. *J. Bacteriol.* **192**, 5881-5886 (2010).

41. P. Mahinthichaichan, D. M. Morris, Y. Wang, G. J. Jensen, E. Tajkhorshid, Selective permeability of carboxysome shell pores to anionic molecules. *J. Phys. Chem. B* **122**, 9110-9118 (2018).

42. A. Hassanali, F. Giberti, J. Cuny, T. D. Kühne, M. Parrinello, Proton transfer through the water gossamer. *Proc. Natl. Acad. Sci. USA* **110**, 13723-13728 (2013).

43. M. R. Badger, Kinetic properties of ribulose 1,5-bisphosphate carboxylase/oxygenase from Anabaena variabilis. *Arch. Biochem. Biophys.* **201**, 247-254 (1980).

44. M. R. Badger, G. D. Price, CO_2 concentrating mechanisms in cyanobacteria: molecular components, their diversity and evolution. *J. Exp. Bot.* **54**, 609-622 (2003).

45. M. R. Badger, T. D. Sharkey, S. von Caemmerer, The relationship between steady-state gas exchange of bean leaves and the levels of carbon-reduction-cycle intermediates. *Planta* **160**, 305-313 (1984).

46. J. Spitzer, B. Poolman, How crowded is the prokaryotic cytoplasm? *FEBS Lett.* **587**, 2094-2098 (2013).

47. M. Tabaka, T. Kalwarczyk, J. Szymanski, S. Hou, R. Holyst, The effect of macromolecular crowding on mobility of biomolecules, association kinetics, and gene expression in living cells. *Frontiers in Physics* **2** (2014).

48. A. Akole, J. M. Warner, Model of influenza virus acidification. *PLoS One* **14**, e0214448 (2019).

49. J. F. Viso *et al.*, Multiscale modelization in a small virus: Mechanism of proton channeling and its role in triggering capsid disassembly. *PLoS Comput. Biol.* **14**, e1006082 (2018).

50. M. Eisenhut *et al.*, The plant-like C2 glycolate cycle and the bacterial-like glycerate pathway cooperate in phosphoglycolate metabolism in cyanobacteria. *Plant Physiol.* **142**, 333-342 (2006).

51. M. R. Badger *et al.*, The diversity and coevolution of Rubisco, plastids, pyrenoids, and chloroplast-based CO_2-concentrating mechanisms in algae. *Can. J. Bot.* **76**, 1052-1071 (1998).

52. R. M. L. McKay, S. P. Gibbs, K. C. Vaughn, RuBisCo activase is present in the pyrenoid of green algae. *Protoplasma* **162**, 38-45 (1991).

53. G. D. Price, D. Sültemeyer, B. Klughammer, M. Ludwig, M. R. Badger, The functioning of the CO_2 concentrating mechanism in several cyanobacterial strains: a review of general physiological characteristics, genes, proteins, and recent advances. *Can. J. Bot.* **76**, 973-1002 (1998).

710 54. S. Hoops *et al.*, COPASI—a COmplex PAthway SImulator. *Bioinformatics* **22**, 3067-3074 (2006).
712 55. L. Whitehead, B. M. Long, G. D. Price, M. R. Badger, Comparing the *in vivo* function of α-carboxysomes and β-carboxysomes in two model cyanobacteria. *Plant Physiol.* **165**, 398-411
714 (2014).
56. S. M. Whitney, P. Baldet, G. S. Hudson, T. J. Andrews, Form I Rubiscos from non-green algae
716 are expressed abundantly but not assembled in tobacco chloroplasts. *Plant J.* **26**, 535-547 (2001).
718 57. A. Occhialini, M. T. Lin, P. J. Andralojc, M. R. Hanson, M. A. J. Parry, Transgenic tobacco plants with improved cyanobacterial Rubisco expression but no extra assembly factors grow at
720 near wild-type rates if provided with elevated CO_2. *Plant J.* **85**, 148-160 (2016).
58. B. M. Long *et al.*, Carboxysome encapsulation of the CO_2-fixing enzyme Rubisco in tobacco
722 chloroplasts. *Nat. Commun.* **9** (2018).
59. G. Zhu, R. J. Spreitzer, Directed mutagenesis of chloroplast ribulose-1,5-bisphosphate
724 carboxylase/oxygenase: Loop 6 substitutions complement for structural stability but decrease catalytic efficiency. *J. Biol. Chem.* **271**, 18494-18498 (1996).
726 60. R. J. Spreitzer, S. R. Peddi, S. Satagopan, Phylogenetic engineering at an interface between large and small subunits imparts land-plant kinetic properties to algal Rubisco. *Proc. Natl.
728 Acad. Sci. USA* **102**, 17225-17230 (2005).